

DR. MASAKAZU YASHIRO (Orcid ID : 0000-0001-5743-7228)

Article type : Research Article

## Absorbed dose distributions from beta-decaying radionuclides: experimental validation of Monte Carlo tools for radiopharmaceutical dosimetry

Ashok Tiwari, and John Sunderland<sup>a)</sup>

*Department of Radiology, University of Iowa Hospitals and Clinics, 200 Hawkins Dr., Iowa City, IA 52242-1077, USA*

*Department of Physics, University of Iowa, 203 Van Allen Hall, Iowa City, IA 52242-1479, USA*

Stephen A. Graves

*Department of Radiology, University of Iowa Hospitals and Clinics, 200 Hawkins Dr., Iowa City, IA 52242-1077, USA*

*Department of Radiation Oncology, University of Iowa Hospitals and Clinics, 200 Hawkins Dr., Iowa City, IA 52242-1089, USA*

Sarah Strand and Ryan Flynn

*Department of Radiation Oncology, University of Iowa Hospitals and Clinics, 200 Hawkins Dr., Iowa City, IA 52242-1089, USA*

Running title: validation of MC beta dose distributions

a) Author to whom correspondence should be addressed. Electronic mail: john-sunderland@uiowa.edu

Department of Radiology, University of Iowa Hospitals and Clinics, 200 Hawkins Drive, Iowa City, IA, 52242 USA

This article has been accepted for publication and undergone full peer review but has not been through the copyediting, typesetting, pagination and proofreading process, which may lead to differences between this version and the [Version of Record](#). Please cite this article as [doi: 10.1002/MP.14463](#)

This article is protected by copyright. All rights reserved

## Abstract

**Purpose:** This study aims to experimentally validate the Monte Carlo generated absorbed doses from the beta particles emitted by  $^{90}\text{Y}$  and  $^{177}\text{Lu}$  using radiochromic EBT3 film-based dosimetry.

**Methods:** Line sources of  $^{90}\text{Y}$  and  $^{177}\text{Lu}$  were inserted longitudinally through blocks of low-density polyethylene and tissue-equivalent slabs of cortical bone and lung equivalent plastics. Radiochromic film (Gafchromic EBT3) was laser-cut to accommodate orthogonal line-sources of radioactivity, and the film was sandwiched intimately between the rectangular blocks to achieve charged particle equilibrium. Line sources consisted of plastic capillary tube of length  $(13 \pm 0.1)$  cm, with 0.42 mm inner diameter and a wall thickness of 0.21 mm.  $^{90}\text{Y}$  line sources were prepared from a solution of dissolved  $^{90}\text{Y}$  resin microspheres.  $^{177}\text{Lu}$  line sources were prepared from an aliquot of  $^{177}\text{Lu}$ -DOTATATE. Film exposures were conducted for durations ranging from 10 minutes to 38 hours. Radiochromic film calibration was performed by irradiation with 6 MV bremsstrahlung x-rays from a calibrated linear accelerator, in accordance with literature recommendations. Experimental geometries were precisely simulated within the GATE Monte Carlo toolkit, which has previously been used for the generation of dose point kernels.

**Results:** The mean percentage difference between measured and simulated absorbed doses were 5.04% and 7.21% for  $^{90}\text{Y}$  and  $^{177}\text{Lu}$  beta absorbed dose in the range of (0.1 -10)Gy. Additionally, 1D gamma analysis using a local 10%/1 mm gamma criterion was performed to compare the absorbed dose distributions. The percentage of measurement points passing the gamma criterion, averaged over all tests, was 93.5%.

**Conclusions:** We report the experimental validation of Monte Carlo derived beta absorbed dose distributions for  $^{90}\text{Y}$  and  $^{177}\text{Lu}$ , solidifying the validity of using Monte Carlo-based methods for estimating absorbed dose from beta emitters. Overall, excellent agreement was observed between the experimental beta absorbed doses in the linear region of the radiochromic film and the GATE Monte Carlo simulations demonstrating that radiochromic film dosimetry has sufficient sensitivity and spatial resolution to be used as a tool for measuring beta decay absorbed dose distributions.

Key words: absorbed dose, dosimetry, GATE Monte Carlo, Gafchromic film EBT3

## 1. INTRODUCTION

Targeted radionuclide therapy (TRT) is a rapidly developing area in nuclear medicine that is demonstrating paradigm shifting treatment efficacy across a number of cancers.<sup>1</sup> It is becoming increasingly clear that effectiveness of TRT could be substantially enhanced through the implementation of image-based personalized dosimetry, which would allow modulation of treatment doses designed to optimize treatment to tumors, while keeping absorbed doses to critical organs below toxicity thresholds.<sup>2,3</sup> The dose point kernel (DPK) method has recently gained considerable attention because of its potential to use image-based information for the calculation of absorbed dose in patient-specific targeted radionuclide therapy.<sup>4</sup> Using the radionuclide specific DPKs, one can perform voxel level dose calculations for estimation of critical organ absorbed dose to avoid patient toxicity, or tumor absorbed dose to better estimate efficacy.<sup>5</sup> However, for multiple reasons, this method is not yet routinely implemented in clinical settings<sup>6</sup>.

The current gold standard for 3D voxelwise dosimetry is personalized, patient-specific Monte Carlo calculations using the quantitative nuclear imaging distributions (SPECT or PET) as the input data for the absorbed dose deposition map. Monte Carlo simulations are, however, highly computationally intensive, if one wants to achieve low statistical noise at the voxel level.<sup>4,7</sup> The DPK method<sup>8</sup> is a more computationally efficient approach and is more typically used in dosimetry software applications, such as MIM, DOSIsoft and Velocity. This method uses pre-calculated, radionuclide- and tissue-specific DPKs and image-based patient specific radionuclide distributions as input data to generate patient-specific absorbed dose maps. In each of these cases, the pre-tabulated DPKs are also based upon Monte Carlo-based calculations. To assess a patient's absorbed dose rate, the radionuclide distribution, as determined by imaging, is convolved with the radionuclide specific DPK to achieve a patient specific dose map. DPKs can be defined as energy deposition kernels from point isotropic radioactive sources. DPKs have been generated by many authors analytically as well as using different Monte Carlo codes.<sup>9-16</sup>

Over the last few decades, there has been growing interest in the measurement of absorbed doses from internal emitters such as <sup>90</sup>Y, <sup>177</sup>Lu, <sup>111</sup>In, and <sup>131</sup>I radionuclides in molecular radiotherapy. First measurement of absorbed dose by beta-emitting radionuclides were performed in 1986 by using miniature thermoluminescent dosimeter (TLD).<sup>17</sup> TLDs have been used in phantoms for the absorbed dose contribution from gamma radiation in the  $\beta^-$  decay of <sup>131</sup>I absorbed dose measurements<sup>18,19</sup> and <sup>111</sup>In gamma absorbed dose<sup>20</sup> where submillimeter resolution is not critical. Polymer gel has also been utilized to test the suitability for <sup>131</sup>I absorbed dose measurements<sup>21</sup>. In the last few years, radiochromic film has been used for verification of external beam dosimetric accuracy<sup>22</sup>, for IMRT dose verification<sup>23</sup>, feasibility of alpha-particle dosimetry<sup>24</sup> and

dose calibration for Ir-192 brachytherapy.<sup>25</sup> In addition, radiochromic film has been employed for the measurement of the absolute activity for high-energy beta emitters.<sup>26</sup> The dosimetric approach of using radiochromic film may be suitable for our aim of measuring beta absorbed doses due to its inherently high spatial resolution, minimal absorbed dose-rate and energy independence, and its near tissue equivalence from an atomic composition standpoint.

One fundamental limitation to using this DPK method in clinical dosimetry is that the dose kernels are based upon analytic or numerical calculations, or Monte Carlo simulations of beta absorbed dose deposition, yet, these probabilistic physics-based energy deposition calculations have not, to date, been experimentally validated. The lack of experimental validation work in the literature is primarily due to the challenge of accurately measuring absorbed dose deposition along the relatively short beta range of therapeutic radionuclides (1 – 10 mm) with sufficient spatial resolution to meaningfully compare with Monte Carlo simulations.

The goal of this work was to validate Monte Carlo-based dosimetry estimates in different tissue types for the commonly used therapeutic radionuclides – <sup>90</sup>Y and <sup>177</sup>Lu. In this work we describe an innovative technique for high-resolution dosimetry of  $\beta^-$  particles using radiochromic film. The significance of this work is that it will provide direct, experimentally-derived evidence regarding the accuracy of Monte Carlo-based dosimetric calculations and provide a range of experimental uncertainty in radionuclide film-based dosimetry.

## 2. MATERIALS AND METHODS

Gafchromic EBT3 radiochromic film offers sensitivity in the 0.1–10 Gy dose range.<sup>27</sup> The film is comprised of an active layer, nominally 28  $\mu\text{m}$  thick, sandwiched between two 125  $\mu\text{m}$  polyester substrates. When EBT3 film is exposed to ionizing radiation, it reacts to form a blue colored polymer with absorption maxima at approximately 635 nm.<sup>28</sup> The effective atomic number ( $Z_{\text{eff}}$ ) of the active layer of this film is 7.26, which is close to the  $Z_{\text{eff}}$  of water (7.42). The spatial resolution is sub-mm when read-out by conventional flatbed scanners.<sup>22</sup> As a self-developing film, EBT3 film requires no post-processing to develop or fix the image. Film handling protocols provided by AAPM Task Group 55 were meticulously followed in this work.<sup>29</sup> Powder-free latex gloves were used while handling film to minimize surface contamination. Light exposure was minimized by handling the films in opaque envelops before and after exposure. Films were stored in a temperature and humidity-controlled environment. The orientation of films during scanning was held constant for all experimental and calibration films.

### 2.1. Film and Phantom Preparation

Calibration films were prepared by cutting EBT3 film into square pieces of dimension  $\sim 3.8 \times 3.8 \text{ cm}^2$  using a guillotine cutter. With this cutting technique, the film layers separate near the cut edges. For our purposes this is acceptable, as we were able to avoid the measurements near the edges. Experimental films used for beta absorbed dose measurements were prepared by laser-cutting square pieces of dimension  $4 \times 4 \text{ cm}^2$  with a central hole of diameter 0.88 mm. The central hole was precisely sized to snugly insert the cylindrical line source of diameter 0.84 mm. Laser cutting was performed using a KERN laser cutting system with the following settings: black vector color enabled with the laser speed of 2 inches/second, 10 % power, 7500 Hz frequency, EMF import with  $\pm 4\%$ , and tool offset of  $\pm 3.5\%$ . All films used in this work were prepared from a single lot number to mitigate potential changes in film sensitivity. A CNC milling machine was used for the phantom drilling processes with the drill size of 0.88 mm diameter. The same drill size was used for all phantom slabs drilling.

The tissue-equivalent materials used for the phantoms were designed to be larger than the maximum  $\beta^-$  range within each material. Three different tissue-equivalent materials were utilized – low-density polyethylene ( $\rho = 0.940 \text{ g/cm}^3$ ), cortical bone tissue equivalent ( $\rho = 1.898 \text{ g/cm}^3$ ) and lung equivalent material ( $\rho = 0.307 \text{ g/cm}^3$ ). The low-density polyethylene cylindrical disk employed in this work had a thickness and radius of 2 cm. Cortical bone and lung equivalent materials had a thickness of 2 cm and dimensions of  $5 \times 5 \text{ cm}^2$ . Tissue-equivalent materials (cortical bone, 05750107 - 19F2 -212; lung tissue, 05750111- LG3 -145) were purchased from CIRS (Computerized Imaging Reference Systems, Inc. 2019).

## 2.2. Film Calibration and Scanning Protocol

The same lot number of Gafchromic EBT3 film that were used in the  $\beta^-$  absorbed dose experiments were separately calibrated using standard techniques. Specifically, the  $3.8 \times 3.8 \text{ cm}^2$  square films were irradiated individually by a 6 MV photons beam by using a calibrated linear accelerator (Siemens Oncor). The photons irradiations were performed at a source-to-surface distance (SSD) of 100 cm, with a  $10 \times 10 \text{ cm}^2$  field (defined at the surface), and at a depth of 10 cm in a solid water. Solid water phantom was added below the EBT3 film to provide the necessary back-scatter. The number of monitor units (MU) used during irradiation were 0, 10, 20, 30, 50, 70, 100, 150, 200, 250, 300, 400, 500, 600, 800, 1000, 1400 and 2000 MU. The reference absorbed doses corresponding to these MUs were 0, 0.07, 0.13, 0.20, 0.34, 0.47, 0.67, 1.01, 1.34, 1.68, 2.01, 2.68, 3.35, 4.02, 5.36, 6.70, 9.38 and 13.40 Gy. Optical scanning of calibration films was performed 24 h post-exposure in order to let the polymerization process stabilize and have all films scanned at the same level of post-exposure growth.<sup>29</sup> Films were scanned (Epson 12000XL: 508 dpi, RGB format, 48-bit, TIFF image format, reflective

mode, no color corrections) one at a time using a positioning jig with consistent orientation as recommended for radiochromic film dosimetry.<sup>30,31</sup>

Film measurements were fit to a rational function to obtain the calibration curves. Dose-response curves were obtained by using the three-parameter function given by,

$$X(D) = \frac{b + D}{a + Dc} \quad \dots \dots \dots \quad (1)$$

where X(D) is the scanner response, D is absorbed dose, and a, b, and c are constants. The fitting parameters a, b, and c are different for different each color channel, which are necessary to convert the film response to the dose map.

### 2.3. Line Source Preparation

Typically, the dose point kernels are calculated using an isotropic point source in a homogeneous media. However, the difficulty of reproducibly creating a point source of known absolute activity, coupled with the point source having the concentration necessary to achieve linear absorbed doses (0.1-10 Gy) was prohibitive. The line sources consisted of the plastic capillary tube of length ( $13 \pm 0.1$ ) cm, having a 0.42 mm internal diameter with a wall thickness of 0.21 mm. Attenuation in the tubing wall, regardless of how thin, will impact the beta spectra seen by the film, however, the tubing geometry and material was precisely simulated in the Monte Carlo simulations. A 27-gauge syringe was used to inject the activity solution in the capillary tube that was sealed at both ends to prevent the leakage during the experiment.

$^{90}\text{Y}$  line sources were prepared by dissolving the  $^{90}\text{Y}$ -SIR microspheres as described by Lourenco et al.<sup>32</sup> First, a 30 ml 0.03 M  $\text{Fe}^{3+}$  stock solution in 1.5 M  $\text{HNO}_3$  was prepared. The supernatant was removed from a vial of SIR-Spheres leaving a reduced volume of ~1 mL. 38  $\mu\text{l}$  of the iron stock solution was added. The vial was left for 15 min to allow for binding of  $\text{Fe}^{3+}$  to sulfonated functional groups. 200  $\mu\text{l}$  of  $\text{H}_2\text{O}_2$  (30 wt%) was then added to the microsphere solution to reach a final concentration of ~6%  $\text{H}_2\text{O}_2$ . The vial was heated to 80 °C for 60 min and was left to cool for 15 min. Subsequently, 30  $\mu\text{l}$   $\text{Fe}^{3+}$  in 8 M  $\text{HNO}_3$  was added to the mixture to reach 1 M  $\text{HNO}_3$  in the solution. Sphere digestion was complete, with a final concentration of 316 MBq/ml concentration and was used to fill the line sources, resulting in a final activity in the tube of ( $0.336 \pm 0.015$ ) MBq/cm at the beginning of the experiment.

For  $^{177}\text{Lu}$ , a suitable volume of activity was taken from a vial of  $^{177}\text{Lu}$ -DOTATATE. An activity concentration of 333 MBq/ml was used to fill the line sources, and the final activity per unit length in the tube was ( $0.355 \pm 0.014$ ) MBq/cm prior to irradiating the films.

### 2.4. Film Exposure

Film was sandwiched between two pieces of phantom material and the line source was placed along the central axis of the phantom (Figure 1). Films were exposed for different durations (10 minutes – 38 hours) to assure that we had films with exposures in the linear dose range of the film 0.1 - 10 Gy at different radii. Experimental films were scanned using identical methods matching that of the calibration films, and images were converted to a dose map for each color channel using the calibration curves.  $^{90}\text{Y}$  exposures were performed for 10 minutes to 24 hours in three different tissue types. Experiments with  $^{177}\text{Lu}$  were only performed using the lung equivalent material for 6 to 38 hours because of its short range in low-density polyethylene and cortical bone.

## 2.5. Absorbed Dose Calculations

Absorbed dose in films was calculated using the calibration function. The calibration function was inverted, and absorbed doses were calculated using the fitting parameters for different channels. The background reading in beta-exposed films was calculated by comparing the mean optical density against that of three unexposed films. This measured background was subtracted from resultant beta absorbed dose distribution measurements. Origin of the images, i.e., the center of each line source, were picked by using the MATLAB *getpts* function. Coordinates of the origin of these images were obtained by using the weighted mean of set of six different measurements. The 1D absorbed dose distribution was then obtained by using the volume averaging of the pixel values with cumulative bin sizes. The mean value of the absorbed dose deposition on the red and the green channel were used to calculate the beta absorbed dose.

The red channel is usually used to ensure dosimetric quality using a conventional fraction dose because the red channel is more accurate at absorbed doses within 4 Gy than the green channel.<sup>33</sup> However, the red channel is prone to rapid degradation of sensitivity at higher absorbed doses, while degradation of the green channel is slow. In this study, the dual channel method using the red and green channel was used for the beta absorbed dose calculations in the range of 0.1 - 10 Gy.

## 2.6. Sources of uncertainty in measurement of absorbed dose

Clinically, an overall standard uncertainty of <10% is desirable. Therefore, to calculate whether the measured absorbed doses are in legitimate window, the uncertainty budget in experimental measurement of absorbed doses were analyzed. A complete portrait of primary sources of uncertainty in absorbed dose measurement are provided. Overall uncertainties in absorbed dose were calculated based on the following components:

### 2.6.1. Uncertainty in calibration irradiations and curve fitting parameters

The uncertainty budget due to calibration of the films comprised of the uncertainties in background measurement of the film, scanner/film response, curve fitting parameters and due to the uncertainties in irradiation process during the film calibration. The clinical linac employed for the film calibration had an uncertainty in output within 2% ( $k=1$ ) of absolute truth<sup>34</sup>. To measure the uncertainties in fitting parameters the equation (1) was used, where the quantity  $X(D)$  represents the net optical density. Equation (1) can be re-written as,

$$D = \frac{b - aX(D)}{cX(D) - 1} \dots\dots\dots (2)$$

Let us now express the net optical density mathematically as:

$$\begin{aligned} X(D) &= OD_{exposed\_film} - OD_{unexposed\_film} \\ &= \log_{10} \frac{I_{unexp} - I_{bckg}}{I_{exp} - I_{bckg}} \dots\dots\dots (3) \end{aligned}$$

Now, the uncertainty propagation associated with the net optical density is<sup>35</sup>,

$$\sigma_{X(D)} = \frac{1}{\ln 10} \sqrt{\frac{\sigma_{I_{unexp}}^2 + \sigma_{I_{bckg}}^2}{(I_{unexp} - I_{bckg})^2} + \frac{\sigma_{I_{exp}}^2 + \sigma_{I_{bckg}}^2}{(I_{exp} - I_{bckg})^2}} \dots\dots\dots (4)$$

where,  $I_{unexp}$  is intensity value of unexposed films,  $I_{exp}$  is intensity value of exposed films i.e., scanner-read out of exposed films,  $I_{bckg}$  is the zero-light transmitted intensity value measured with the opaque piece of film, and  $\sigma_{I_{unexp}}$ ,  $\sigma_{I_{exp}}$  and  $\sigma_{I_{bckg}}$  are corresponding standard deviations in unexposed, exposed and background intensity measurements. It should be noted that all quantities in equations (3) and (4) were calculated over the same ROI drawn on the film. For simplicity, cross-correlations between fit parameters and the uncertainty on measured optical density were ignored. A simple expression for uncertainty propagation can now be written as:

$$\sigma_y^2 = \sum_i \left( \frac{\partial y}{\partial x_i} \right)^2 \sigma_{x_i}^2 \dots\dots\dots (5)$$

where,  $i = a, b, c$  for three fitting parameters and  $\sigma_{x_i}$  represents the uncertainties in fitting parameters. After calculating the partial derivatives of each term using the equation (2) and substituting in equation (5), we can get the variance in absorbed dose:

$$\sigma_{D_{fitting}}^2 = \frac{X(D)^2}{(cX(D) - 1)^2} \sigma_a^2 + \frac{1}{(cX(D) - 1)^2} \sigma_b^2 + \frac{X(D)^2 (b - aX(D))^2}{(cX(D) - 1)^2} \sigma_c^2$$

Therefore, the total absorbed dose uncertainty due to curve fitting becomes,

$$\sigma_{D_{fitting}} = \sqrt{\frac{X(D)^2 \sigma_a^2 + \sigma_b^2 + X(D)^2 (b - aX(D))^2 \sigma_c^2}{(cX(D) - 1)^2}} \dots\dots\dots (6)$$

### 2.6.2. Uncertainty propagation in experimental irradiations

Uncertainty in exposure time and film irradiation contributes the uncertainties propagation in experimental irradiations. Exposure time uncertainties were minimized by quick changing and loading a new film after exposure and clock was used to keep record of the exposures. For (4-38) hours of exposure, exposure time had a maximum permissible uncertainty of  $\pm 2$  minutes. Films take out after the exposure and loading a new film are accounted by the uncertainty in the film exposure. Absolute propagated uncertainty in absorbed dose ( $D$ ) can be calculated by taking the derivative both sides in equation (2) with respect to  $X(D)$  and simplifying, we get,

$$\frac{dD}{dX(D)} = \frac{-bc}{(cX(D) - 1)^2} + \frac{a}{(cX(D) - 1)^2} = \frac{a - bc}{(cX(D) - 1)^2}$$

Therefore, uncertainty in measured absorbed dose given by equation (2) is,

$$\sigma_{D_{exp}} = \sigma_{X(D)} \left| \frac{a - bc}{(cX(D) - 1)^2} \right| \dots\dots\dots(7)$$

where,  $\sigma_{X(D)}$  is the uncertainties in net optical density.

### 2.6.3. *Uncertainty propagation in activity concentration measurement*

A Dose calibrator was used to measure the activity of  $^{90}\text{Y}$  and  $^{177}\text{Lu}$  sources. Activity measurements were assigned an uncertainty of  $\sim 5\%$ . First, the source vial was weighed, and the activity was transferred to the syringe. The vial was re-weighed to calculate the mass difference to determine volume. The residual vial activity was re-assayed to calculate the activity difference. The activity and volume data were utilized to calculate the activity concentration. Uncertainties in concentration associated with activities and volumes were propagated in quadrature.

## 2.7. Monte Carlo Simulations

Experimental irradiations, including the exact phantom geometry with the Gafchromic film, were simulated in the Monte Carlo platform to determine the energy deposition by the beta decay of radionuclides. All layers of the film were simulated using the density and atomic compositions of the film active layer and matte-polyester layer given in Appendix Table 1. GATE (GEANT4 Application for Tomographic Emission) is the Monte Carlo simulation toolkit which encapsulates the GEANT4 libraries.<sup>36</sup> In this work, GATE version 8.1 was used for all simulations. The Geant4 “ion” source was used to generate the  $\beta^-$  decay spectrum of  $^{90}\text{Y}$ . For  $^{177}\text{Lu}$ , the beta spectrum including the conversion electrons were simulated using the spectra from MIRD data<sup>37</sup>. Using the ion source of  $^{90}\text{Y}$ ,  $\sim 1$  million events were simulated in 1 hour, while using  $^{177}\text{Lu}$  spectrum source,  $\sim 2.4$  million events were simulated. Absorbed dose deposition was tabulated in cylindrical concentric shells with height of

voxel size in the longitudinal axis around a line source at fixed radial distances. The thickness of the tally shells was made to be equal to the voxel size (0.05 mm) of the 3D simulation matrix. The origin of the polar coordinate system ( $r, \theta$ ) was positioned at the center of the experimental films. The electromagnetic (EM) constructor called *emstandard\_opt3* was implemented for the physics list within GATE. This EM constructor is useful for applications that require higher accuracy of electrons, hadrons, and ion tracking.<sup>38</sup> In GATE, *doseActor* was used to calculate the energy deposition. The deposited energy *EDep* was scored at the voxel level, and associated uncertainties were calculated in each voxel with the doseActor *Uncertainty EDep*.<sup>39</sup>

## 2.8. Quantification of absorbed dose distributions: the gamma index test

To quantify the observed level of agreement between the measured and simulated absorbed dose distributions, the  $\gamma$ -index dose comparison method was implemented.<sup>40,41</sup> Instead of using the dose difference (DD) and distance-to-agreement (DTA) criteria separately, this method combines both metrics into a single  $\gamma$ -index. In this work, the dose-difference distribution was computed, point-by-point to co-locate the measured absorbed dose distribution and the simulated distribution. To perform this gamma function test, the absorbed dose and distance criteria were fixed using preselected values. In practice, the values can be set as functions of space or absorbed dose value. In this work, an acceptable tolerance of 10% as a dose-difference ( $\Delta D$ ) and 1mm distance-to-agreement ( $\Delta d$ ) criterion was set. The selection of gamma criteria was based on the measurement uncertainty, and beta particles range in different tissues under consideration. However, the DTA of 1 mm is not quite adequate for better comparison of <sup>177</sup>Lu emitted beta absorbed dose distribution because of its small range, but it is the best from a measurement perspective. Using this method points with  $\gamma < 1$  are defined as passing preset tolerances and vice versa. The gamma index at a point  $r_s$  is defined as:

$$\gamma(r_s) = \min(\Gamma(r_s, r_m)) \forall \{r_m\}$$

where

$$\Gamma(r_s, r_m) = \sqrt{\frac{\delta^2(r_s, r_m)}{\Delta D^2} + \frac{r^2(r_s, r_m)}{\Delta d^2}} \quad \dots\dots\dots (8)$$

where  $\delta(r_s, r_m)$  is the dose difference between simulated and measured absorbed doses at point  $r$ ,  $\Delta D$  is the dose difference criterion,  $r(r_s, r_m)$  is euclidean distance between simulated and measured absorbed dose points, and  $\Delta d$  is the distance-to-agreement criterion. The gamma index method implemented in this work used the local gamma normalization where the  $\Delta D$  is normalized to the local maximum value.

## 3. RESULTS

### **3.1. Film Calibration**

The scanned calibration films (Figure 2) were decomposed into red, green, and blue channels for data analysis. For each calibration film, an ROI of  $5 \times 5 \text{ mm}^2$  in the center of the film was analyzed to determine the mean pixel value vs. the delivered dose. Calibration was performed for each color channel separately. The fitting function given by equation (1) was found to best fit the calibration data, showing an  $R^2$  coefficient  $> 0.999$  for all three channels with the expected absorbed dose. Uncertainties in fitting parameters were found to be less for the red channel at  $(2.20 \pm 1.02)\%$ , whereas errors were comparable for the green and blue channel at  $(4.32 \pm 1.28)\%$ .

The correlation between the intensity of the three-color channels RGB of the scanned image and the absorbed dose represents the calibration curve. Pixel values were plotted as a function of absorbed dose and fitted by a rational function defined by equation (1). The calibration curves are shown in Figure 3. Clearly the dynamic range of the film was observed in the calibration curve. The red and green channels exhibited the highest sensitivity, i.e., the net optical density per unit dose, whereas the blue color channel was found to be least sensitive in terms of dose-response. Consequently, the blue channel dose was excluded in all calculations throughout the analysis. The average uncertainty in absorbed dose was  $(2.80 \pm 0.52)\%$ ,  $(3.62 \pm 1.26)\%$ ,  $(4.91 \pm 1.51)\%$  for the red, green, and blue channels, respectively. The dual (red and green) channel dosimetry algorithm was implemented in an in-house MATLAB R2016a code.

### **Experimental films exposure with line sources: experiment**

Three sets of 8 EBT3 experimental films were exposed to  $^{90}\text{Y}$  line source with exposures of 10, 30 minutes, 1, 2, 4, 8, 16, and 24 hours using the low-density polyethylene, cortical bone and lung equivalent phantoms. Using  $^{177}\text{Lu}$ , films were exposed only in lung equivalent slabs with exposure times of 6, 12, 16 and 38 hours (Figure 4).

### **3.2. Absorbed dose uncertainty estimates**

The primary components of uncertainty in an absorbed dose measurement has been examined. The total uncertainties in optical densities for red, green, and blue channels were  $(0.78 \pm 0.62)\%$ ,  $(0.80 \pm 0.73)\%$  and  $(0.94 \pm 0.76)\%$  respectively. For the absorbed dose measurements using the red and green channel at absorbed doses ranging from (0 - 10) Gy, a combined total uncertainty of  $(4.56 \pm 1.35)\%$  was obtained, but the red channel exhibited a lower total uncertainty of  $(2.80 \pm 0.52)\%$ . The experimental uncertainties were comparable

to the combined uncertainty arising due to the fitting process. Uncertainties propagated in calibration and experimental procedures are summarized in Table 1.

### 3.3. Experiment vs. Monte Carlo simulations

We were able to measure the absorbed dose in the range of (0.1-10) Gy as a function of radial distances using discrete radial measurements every 0.05mm, as shown in plots presented in Figure 5. Although we irradiated the films for eight different exposure times, only plots belonging to the absorbed dose values that lie in the dynamic range of the film in each tissue type are presented in Figure 5. Above the 16-hours exposure, the beta absorbed dose was saturated and below 4 hours, the absorbed dose was below 0.1 Gy, and therefore not in the linear range of the film. These plots are sufficient to obtain a qualitative assessment of the dose linearity and the absorbed doses in the sensitive region of the EBT3 film. Monte carlo simulations were performed using the experimenal exposure durations as explained in section 2.4. Higher discrepancies were observed proximal to the line source due to the film delamination around the laser-drilled hole, so these data were excluded from the analysis. The average statistical uncertainties in all simulations were less than 4.5% for the absorbed dose range of (0.1–10) Gy. For the beta absorbed dose, the mean point-to-point absolute percentage difference between the MC results and experimental measurements was 5.04% using  $^{90}\text{Y}$  and 7.21% when using the  $^{177}\text{Lu}$  line sources. The percentage difference was calculated down to a absorbed dose value of 0.1 Gy for all exposures, which is the lowest sensitive region of the EBT3 film. Higher deviations were observed for the region that is close to the film and line-source interface, and the lower dose regions, especially close to 0.1 Gy. These disagreements in the lower dose region between the experiment and Monte Carlo simulations are due to the lower signal to noise ratio. The density and atomic composition of the tissue equivalent slabs are needed to reproduce Monte Carlo results described herein, and thus we have included these values in Appendix Table 2.

The  $^{90}\text{Y}$  irradiations, as presented in Figure 5 (A-C) give the  $\beta^-$  absorbed dose as a function of radial distances for different exposure times. The measured absorbed dose shown in Figure 5 (A-C) is the sum of beta and bremsstrahlung component of absorbed doses. As the bremsstrahlung photon range is substantially longer than the size of our phantom, the experimental geometry used in this work does not include all the bremsstrahlung doses beyond the size of the phantom. It should be noted that the range of the  $^{90}\text{Y}$  emitted beta particles in lung is  $\sim$ 35 mm. The geometry of the lung phantom used in this experiment therefore could not have deposited all emitted energies. However, as the goal was to measure the deposited absorbed dose in the range of (0.1 -10) Gy (linear range of the film) and for this dose range, the lung phantom geometry was sufficient. The 0.1 Gy lower limit is well-within the boundaries of the phantom size used. The GATE Monte Carlo simulations of the experimental geometry with a larger phantom radius were performed to separate the

beta and bremsstrahlung doses, as shown in Figure 6. The Monte Carlo simulation show that a radial distance of 10 mm in low-density polyethylene is sufficient to account for the entirety of the pure beta absorbed doses. The beta dose function is higher than that of the bremsstrahlung dose by more than three orders of magnitude at 1 mm in low-density polyethylene. As the distances increase, this ratio decreases to near unity, however, as one approaches to 10 mm. The bremsstrahlung dose predominates beyond the cut-off of the beta dose component showing its importance to tissues in this distance interval. As the ratio of the bremsstrahlung dose and beta dose close to the origin is negligible, the experimental bremsstrahlung dose scored in Figure 5 (A-C) is insignificant for the purposes of absorbed dose validation.

The emission of moderate-energy beta  $\beta^-$  particles from the  $^{177}\text{Lu}$  decay as well as low-energy gamma photons results in a relatively low absorbed dose as shown in measured dose data in Figure 5(D). However, only beta absorbed doses were included in the small phantom volume in the Monte Carlo measurement. Comparison between the two is valid, however, because the photonic contribution of the decay can be ignored, since the photon contribution to absorbed dose is typically  $>1000\times$  smaller than the beta dose in the small geometry of the phantom.

From Figure 5, it is evident that the results are in close conformance with the GATE Monte Carlo simulation results. The average difference between measured data using the EBT3 film and MC simulation is observed to be below 6%. Several factors including lack of uniform exposure to the calibration film during the photon irradiation, film drilling artifacts, phantom drilling process, scanner artifacts, the probability of film scratches during the experiment (measurement noise), and noise in Monte Carlo simulations might cause errors in the spatial dose shifts between two distributions.

### 3.4. Comparison of measured and simulated dose distributions

The 1D local gamma evaluation was performed to compare the simulated and measured beta dose distributions using equation (8). The Gamma index was calculated in absolute dose values using 10%/1mm gamma evaluation criteria for each material type. The gamma calculation search radius was set to the value where absorbed dose was 0.1 Gy.

First, 16-hour exposure data using  $^{90}\text{Y}$  sources in lung tissue up to radial distances of (1.5-15) mm was analyzed. The maximum value of  $\gamma$  was 1.75, corresponding to the maximum value of the dose difference (12.7%). The average value of  $\gamma$  in higher dose gradient region (1.5-5) mm was 0.65. Percentage of points passing the 10%/1 mm gamma criterion in (1.5-5) mm region was 94.36%, while in the region (5-15) mm the

passing percentage was 90%. The average passing rate was 94.0%. The  $\gamma$  - index and the measured and simulated absorbed doses are presented in Figure 7.

In addition, 16-hour exposure in cortical bone up to a distance of 4 mm from the line source was analyzed. Up to the distance of 3.5 mm, all comparison points passed the gamma test, and beyond 3.5 mm, calculation points failed the test as can be seen in Figure 7(B). The maximum value of gamma in (3.5-4) mm distance corresponds to the maximum dose difference (14.5%). The percentage of points passing the 10%/1 mm gamma criterion in (1.5-3.5) mm region is 100%, while in the region (1.5-4) mm average passing rate is 90.9%, which is as expected. For  $^{90}\text{Y}$  in polyethylene, using 4-hour exposure time the gamma passing rate calculated was 95.5%, up to a distance of 4.5 mm. Furthermore, for  $^{177}\text{Lu}$  in lung using the 38-hour exposure time, gamma passing rate was 92.3 %, up to the radius of 2 mm.

In summary, the gamma passing rate for  $^{90}\text{Y}$  in low-density polyethylene, cortical bone, and lung were 95.5%, 90.9% and 94.0% respectively. Additionally, the gamma passing rate for  $^{177}\text{Lu}$  in lung was 93.6%. The percentage of points satisfying the constraint  $\gamma < 1$  shows a minimal difference between different tissue types. Overall, the percentage of points passing the preset tolerances of 10%/1 mm in absorbed dose, averaged over all tests was 93.5%. The 1D gamma index analysis suggests that the measured dose distribution is in close agreement with the simulated dose distribution. These results compare favorably with the gamma passing rates in IMRT, where passing rates are typically around ~ 95%, using the standard gamma criteria of 3%/3mm.

#### 4. DISCUSSION

Radionuclides such as  $^{90}\text{Y}$ , and  $^{177}\text{Lu}$  are being increasingly used in targeted radionuclide therapies. Internal emitter dosimetry has been an area of growing importance in targeted radionuclide therapy, due to the potential to improve therapeutic outcomes under a dosimetry-guided treatment paradigm. Various methods are available to calculate the absorbed dose distributions. In patient-specific dosimetry, the DPKs are gaining popularity and are implemented in 3D image-based dosimetry.

The analytic or discretized radionuclide-specific DPKs convolved with the activity map of the organ of the patient and combined with density information from the CT scan can result in quantitative dose rate distributions. Extensive tabulations of the dose point kernels in water, and tissue-specific kernels are also available.<sup>13-16,42,43</sup> However, only a few dose distributions have been validated experimentally, and up until now the beta radiation component has been excluded.<sup>18-20</sup> In this work, we experimentally measured the  $^{90}\text{Y}$  beta absorbed doses in low-density polyethylene, cortical bone, lung, and  $^{177}\text{Lu}$  doses in lung using radiochromic

film and tissue-equivalent phantoms. Measured absorbed doses using the film were assessed by comparing to the corresponding Monte Carlo simulations.

Radiochromic EBT3 film appears to be appropriate for the measurement of beta absorbed doses in this experiment because of its minimal absorbed dose rate ( $\sim 1\%$ )<sup>23,44</sup> and energy dependency.<sup>45-47</sup> Studies suggest that the film energy response changes are reasonably constant ( $\sim 1\%$ ) between 100 keV and 10 MeV. Below 100 keV, the film response can vary substantially as a function of energy (20-30%).<sup>45,46</sup> The almost uniform energy dependence suggests that the EBT3 film can be calibrated using a 6 MV photon beam and used for quantitative measurements of absorbed dose in mixed photon and electron radiation fields in energy ranges relevant to this work.

In this work, only beta absorbed dose from  $^{90}\text{Y}$  and  $^{177}\text{Lu}$  were considered. The choice to investigate  $^{90}\text{Y}$  was made for two reasons: (1) is its relatively common usage in radionuclide therapy, and (2) it has a relatively long range in soft tissues and bone. Furthermore,  $^{90}\text{Y}$  is almost pure  $\beta^-$ -emitter, the very low abundance of  $\gamma$  emissions (<0.01%) combined with the low contribution to absorbed dose by bremsstrahlung interactions of the  $\beta^-$  emissions as explained in section 3.3 avoids significant gamma contribution to the measurement. For  $^{177}\text{Lu}$ , approximately 17 % of the decays involve the emission of low-energy gamma photons [ $E_\gamma = 113$  keV (6.23 %) and 208 keV (10.41 %)] in addition to the betas with an  $E_{\beta(\max)}$  of 496.8 keV (79.44 %), 383.9 keV (8.89 %), and 175.5 keV (11.66%)<sup>48</sup>, which may slightly increase absorbed dose within the range of beta energy deposition. For the phantom radius of 2 mm, the  $^{177}\text{Lu}$  photons are expected to contribute approximately  $\sim 1\%$  to the overall energy deposition.<sup>14</sup> Our decision to measure absorbed dose from  $^{177}\text{Lu}$  in only the lung-equivalent material was due to the longer range of betas in lung ( $\sim 8$  mm) compared to other tissue-equivalent materials.

Advantages of the proposed method with respect to state of the art are severalfold. Firstly, this experiment with EBT3 film can be used to perform high-resolution dosimetry of  $\beta^-$  particles of few other beta-emitting radionuclides with end-point ranges of approximately  $> 5$  mm. Additionally, our results indicate that EBT3 film could be effectively used to obtain experimental 2D absorbed dose measurements within activity-filled phantoms. The dynamic range of the Gafchromic EBT3 film is 0.1 – 10 Gy<sup>49</sup>, and the dynamic range of LiF-based microcube TLDs of dimension 1 mm<sup>3</sup> is 10  $\mu\text{Gy}$  – 1 Gy.<sup>50</sup> Therefore, one could also use the TLDs to measure the beta absorbed doses in certain radial distances. However, one cannot perform the high-resolution dosimetry of  $\beta^-$  particles using the microcube TLDs as they are dimensionally larger than, for example, the beta range of  $^{177}\text{Lu}$ . In addition, microcube TLDs pose experimental limitations relating to phantom construction, accurate positioning of the dosimeter, and air/phantom interfaces, thus potentially limiting the measurement accuracy and inter-investigator agreement. Many isotopes such as  $^{177}\text{Lu}$  and  $^{131}\text{I}$  have significant gamma

emissions that contribute to absorbed dose. Therefore, a combination of film and TLDs in larger phantoms may be appropriate to characterize these dosimetric components.

Although laser cutting parameters were optimized to minimize de-lamination near the line source, the first 1-2 mm of radius was still impacted by delamination. This limitation of the measurement technique made it challenging to accurately measure beta absorbed dose deposition from Lu-177, which has a much smaller maximum beta range. Differences between the experimental absorbed dose and simulated dose in the film was primarily attributed to the curve fitting process, activity measurements and the experimental irradiations. Several other reasons such as the difficulty in precisely locating the origin of the film, laser film drilling artifacts, noise on the films during the experiment setup, and statistical errors in Monte Carlo simulations additionally contributed a small portion. It is important to highlight that the selection of the origin of experimental films has a large influence on the result. During the data analysis, the origin was selected using the MATLAB *getpts* function. This function lets the user manually select points within the image. The final origin position within all films was determined by using the mean of six different measurements. The estimated precision of this approach, as estimated by inter-measurement variability, was  $\pm 0.03$  mm.

Our validation experiments have shown that it is feasible to measure the beta absorbed dose experimentally using radiochromic film-based dosimetry. Good agreement was observed between measured absorbed dose distributions and Monte Carlo simulations for all isotopes and phantom materials. This result (1) provides experimental evidence regarding the accuracy of existing Monte Carlo codes and (2) provides an upper bound on the systematic error from Monte Carlo calculations in the context of radionuclide dosimetry.

## 5. CONCLUSIONS

We have presented a novel, inexpensive, and high-resolution experimental method for validation of beta decay dosimetry. Good agreement was observed between the experimental beta absorbed doses compared with the GATE Monte Carlo simulations for line sources of radioactivity in tissue-equivalent materials. Future work will expand these absorbed dose validation methods to other radionuclides and measurement geometries that include gamma dose contributions at larger radii.

## ACKNOWLEDGEMENTS

The authors would like to thank the University of Iowa Department of Physics machine shop staff for their assistance with laser cutting of film. The authors would also like to thank Prof. Daniel E. Hyer for his input on this project.

## CONFLICT OF INTEREST

The authors declare to have no conflict of interest to disclose.

## REFERENCES

1. Knapp FF, Dash A. *Radiopharmaceuticals for Therapy*. Springer; 2016.
2. Garske-Roman U, Sandstrom M, Baron KF, et al. Prospective observational study of Lu-177-DOTA-octreotate therapy in 200 patients with advanced metastasized neuroendocrine tumours (NETs): feasibility and impact of a dosimetry-guided study protocol on outcome and toxicity. *Eur J Nucl Med Mol I*. 2018;45(6):970-988.
3. Ljungberg M, Celler A, Konijnenberg MW, et al. MIRD Pamphlet No. 26: Joint EANM/MIRD Guidelines for Quantitative Lu-177 SPECT Applied for Dosimetry of Radiopharmaceutical Therapy. *J Nucl Med*. 2016;57(1):151-162.
4. Sanchez-Garcia M, Gardin I, Lebtahi R, Dieudonne A. A new approach for dose calculation in targeted radionuclide therapy (TRT) based on collapsed cone superposition: validation with Y-90. *Phys Med Biol*. 2014;59(17):4769-4784.
5. Huizing DMV, de Wit-van der Veen BJ, Verheij M, Stokkel MPM. Dosimetry methods and clinical applications in peptide receptor radionuclide therapy for neuroendocrine tumours: a literature review. *EJNMMI Res*. 2018;8(1):89.
6. Flux GD, Sjogreen Gleisner K, Chiesa C, et al. From fixed activities to personalized treatments in radionuclide therapy: lost in translation? *Eur J Nucl Med Mol Imaging*. 2018;45(1):152-154.
7. Dieudonne A, Hobbs RF, Lebtahi R, et al. Study of the impact of tissue density heterogeneities on 3-dimensional abdominal dosimetry: comparison between dose kernel convolution and direct Monte Carlo methods. *J Nucl Med*. 2013;54(2):236-243.
8. Berger MJ. Distribution of absorbed dose around point sources of electrons and beta particles in water and other media. *J Nucl Med*. 1971;Suppl 5:5-23.
9. Berger MJ. Improved point kernels for electron and beta-ray dosimetry. *US Atomic Energy Commission*. 1973.
10. Prestwich WV, Nunes J, Kwok CS. Beta-Dose Point Kernels for Radionuclides of Potential Use in Radioimmunotherapy. *J Nucl Med*. 1989;30(6):1036-1046.
11. Furhang EE, Sgouros G, Chui CS. Radionuclide photon dose kernels for internal emitter dosimetry. *Med Phys*. 1996;23(5):759-764.
12. Botta F, Mairani A, Battistoni G, et al. Calculation of electron and isotopes dose point kernels with FLUKA Monte Carlo code for dosimetry in nuclear medicine therapy. *Med Phys*. 2011;38(7):3944-3954.

13. Papadimitroulas P, Loudos G, Nikiforidis GC, Kagadis GC. A dose point kernel database using GATE Monte Carlo simulation toolkit for nuclear medicine applications: comparison with other Monte Carlo codes. *Med Phys*. 2012;39(8):5238-5247.
14. Graves SA, Flynn RT, Hyer DE. Dose point kernels for 2,174 radionuclides. *Med Phys*. 2019;46(11):5284-5293.
15. Tiwari A, Graves S, Sunderland J. Measurements of dose point kernels using GATE Monte Carlo toolkit for personalized convolution dosimetry. *J Nucl Med*. 2019;60.
16. Tiwari A, Graves SA, Sunderland J. The Impact of Tissue Type and Density on Dose Point Kernels for Patient-Specific Voxel-Wise Dosimetry: A Monte Carlo Investigation. *Radiat Res*. 2020. doi: 10.1667/RR15563.1.
17. Wessels BW, Griffith MH. Miniature thermoluminescent dosimeter absorbed dose measurements in tumor phantom models. *J Nucl Med*. 1986;27(8):1308-1314.
18. Giap HB, Macey DJ, Bayouth JE, Boyer AL. Validation of a dose-point kernel convolution technique for internal dosimetry. *Phys Med Biol*. 1995;40(3):365-381.
19. Wilderman SJ, Dewaraja YK. Method for fast CT/SPECT-based 3D Monte Carlo absorbed dose computations in internal emitter therapy. *Ieee T Nucl Sci*. 2007;54(1):146-151.
20. Gardin I, Bouchet LG, Assie K, et al. Voxeldose: a computer program for 3-D dose calculation in therapeutic nuclear medicine. *Cancer Biother Radiopharm*. 2003;18(1):109-115.
21. Gear JI, Charles-Edwards E, Partridge M, Flux GD. Monte Carlo verification of polymer gel dosimetry applied to radionuclide therapy: a phantom study. *Phys Med Biol*. 2011;56(22):7273-7286.
22. Reinhardt S, Hillbrand M, Wilkens JJ, Assmann W. Comparison of Gafchromic EBT2 and EBT3 films for clinical photon and proton beams. *Med Phys*. 2012;39(8):5257-5262.
23. Casanova Borca V, Pasquino M, Russo G, et al. Dosimetric characterization and use of GAFCHROMIC EBT3 film for IMRT dose verification. *J Appl Clin Med Phys*. 2013;14(2):4111.
24. Mukherjee B, Gholami YH, Bhonsle U, Hentschel R, Khachan J. A unique alpha dosimetry technique using Gafchromic EBT3 (R) film and feasibility study for an activity calibrator for alpha-emitting radiopharmaceuticals. *Brit J Radiol*. 2015;88(1056).
25. Oare C, Wilke C, Ehler E, Mathew D, Sterling D, Ferreira C. Dose calibration of Gafchromic EBT3 film for Ir-192 brachytherapy source using 3D-printed PLA and ABS plastics. *3D Print Med*. 2019;5(1):3.
26. Fox RA, Barker P, Smart G. The use of GAFchromic film to determine the absolute activity of beta emitters. *Phys Med Biol*. 1999;44(4):833-842.
27. Ashland™ Gafchromic radiotherapy films. <http://www.gafchromic.com/gafchromic-film/radiotherapy-films/EBT/index.asp>. Accessed August 10, 2019.
28. Callens MB, Crijns W, Depuydt T, et al. Modeling the dose dependence of the vis-absorption spectrum of EBT3 GafChromic films. *Med Phys*. 2017;44(6):2532-2543.
29. Niroomand-Rad A, Blackwell CR, Coursey BM, et al. Radiochromic film dosimetry: Recommendations of AAPM Radiation Therapy Committee Task Group 55. *Med Phys*. 1998;25(11):2093-2115.

30. Huet C, Dagois S, Derreumaux S, Trompier F, Chenaf C, Robbes I. Characterization and optimization of EBT2 radiochromic films dosimetry system for precise measurements of output factors in small fields used in radiotherapy. *Radiat Meas.* 2012;47(1):40-49.
31. Papaconstadopoulos P, Hegyi G, Seuntjens J, Devic S. A protocol for EBT3 radiochromic film dosimetry using reflection scanning. *Medical Physics.* 2014;41(12).
32. Lourenco V, Bobin C, Chiste V, et al. Primary standardization of SIR-Spheres based on the dissolution of the (90)Y-labeled resin microspheres. *Appl Radiat Isot.* 2015;97:170-176.
33. Devic S, Tomic N, Soares CG, Podgorsak EB. Optimizing the dynamic range extension of a radiochromic film dosimetry system. *Med Phys.* 2009;36(2):429-437.
34. van der Merwe D, Van Dyk J, Healy B, et al. Accuracy requirements and uncertainties in radiotherapy: a report of the International Atomic Energy Agency. *Acta Oncol.* 2017;56(1):1-6.
35. Devic S, Seuntjens J, Hegyi G, et al. Dosimetric properties of improved GafChromic films for seven different digitizers. *Med Phys.* 2004;31(9):2392-2401.
36. Jan S, Santin G, Strul D, et al. GATE: a simulation toolkit for PET and SPECT. *Phys Med Biol.* 2004;49(19):4543-4561.
37. Eckerman KF, Endo A. *MIRD: Radionuclide Data and Decay Schemes*. 2nd ed: Society of Nuclear Medicine; 2008.
38. Allison J, Amako K, Apostolakis J, et al. Recent developments in GEANT4. *Nucl Instrum Meth A.* 2016;835:186-225.
39. Sarrut D, Bardies M, Boussion N, et al. A review of the use and potential of the GATE Monte Carlo simulation code for radiation therapy and dosimetry applications. *Med Phys.* 2014;41(6).
40. Low DA, Harms WB, Mutic S, Purdy JA. A technique for the quantitative evaluation of dose distributions. *Med Phys.* 1998;25(5):656-661.
41. Low DA, Dempsey JF. Evaluation of the gamma dose distribution comparison method. *Med Phys.* 2003;30(9):2455-2464.
42. Bolch WE, Bouchet LG, Robertson JS, et al. MIRD pamphlet No. 17: The dosimetry of nonuniform activity distributions - Radionuclide S values at the voxel level. *Journal of Nuclear Medicine.* 1999;40(1):11s-36s.
43. Lanconelli N, Pacilio M, Lo Meo S, et al. A free database of radionuclide voxel S values for the dosimetry of nonuniform activity distributions. *Phys Med Biol.* 2012;57(2):517-533.
44. Arjomandy B, Tailor R, Anand A, et al. Energy dependence and dose response of Gafchromic EBT2 film over a wide range of photon, electron, and proton beam energies. *Med Phys.* 2010;37(5):1942-1947.
45. Sutherland JG, Rogers DW. Monte Carlo calculated absorbed-dose energy dependence of EBT and EBT2 film. *Med Phys.* 2010;37(3):1110-1116.
46. Bekerat H, Devic S, DeBlois F, et al. Improving the energy response of external beam therapy (EBT) GafChromicTM dosimetry films at low energies (<= 100 keV). *Med Phys.* 2014;41(2):022101.

47. Sipila P, Ojala J, Kaijaluoto S, Jokelainen I, Kosunen A. Gafchromic EBT3 film dosimetry in electron beams - energy dependence and improved film read-out. *J Appl Clin Med Phys.* 2016;17(1):360-373.
48. National Nuclear Data Center NuDat (Nuclear Structure and Decay Data). <https://www.nndc.bnl.gov/nudat2/>. Accessed December 15, 2019.
49. Lewis D, Micke A, Yu X, Chan MF. An efficient protocol for radiochromic film dosimetry combining calibration and measurement in a single scan. *Med Phys.* 2012;39(10):6339-6350.
50. Thermo Scientific Harshaw TLD Materials and Dosimeters. <https://assets.thermofisher.com/TFS-Assets/LSG/Catalogs/Dosimetry-Materials-Brochure.pdf>. Accessed December 20, 2019.

Figure 1: (A-C) GATE Monte Carlo simulation set-up with the line source and EBT3 film and (D) experimental setup.

Figure 2: Scanned images of calibration films irradiated with 6MV photon beams.

Figure 3: Sensitometric response curves for the red, green, and blue channels of scanned EBT3 film irradiated by 6MV photons to absorbed dose from 0 to 13.4 Gy using the equation (1). Uncertainties due to the curve fitting process were  $(2.20 \pm 0.86)$  %,  $(3.61 \pm 1.27)$  %, and  $(4.22 \pm 1.58)$  %, for red, green, and blue channels, respectively.

Figure 4: (A) Scanned images of the  $^{90}\text{Y}$  exposed experimental films in low-density polyethylene (first row), cortical bone (second row), and lung equivalent (third row) phantom material. (B): Scanned images of the  $^{177}\text{Lu}$  exposed experimental films in lung equivalent phantom material.

Figure 5: (A-C) Experimental vs. Monte Carlo absorbed dose measurements of  $^{90}\text{Y}$  in polyethylene, cortical bone and lung equivalent phantoms and (D)  $^{177}\text{Lu}$  in lung equivalent phantom for different exposure times. The shaded area corresponds to error bars in simulated and measured absorbed doses. Significant disagreement at small radii is due to delamination of films at the line-source interface.

Figure 6: Monte Carlo simulation of absorbed dose distribution from beta and bremsstrahlung radiation of the decay scheme of  $^{90}\text{Y}$  as a function of distance from a line source of activity 5.18 MBq in a plastic cylinder of wall thickness of 0.21 mm and internal diameter of 0.42 mm using the same line source and similar Monte Carlo setup but with the larger low-density polyethylene geometry of radius of 42 cm. Acquisition time in simulation was 4 hr. The voxel size used for betas simulation was 0.05 mm, whereas for bremsstrahlung simulation was 1 mm. The yellowish shaded region in the plot represents the sensitive region of the EBT3 film.

Accepted Article

Figure 7: 1D  $\Gamma$  analysis calculations for  $^{90}\text{Y}$  simulation and experimental absorbed dose comparisons in (A) lung and (B) cortical bone for 16 hour exposures. The dashed-line in plot is the boundary of the pass-fail region.

Table 1: Various uncertainty components in the experimental work to absorbed dose measurements.

Uncertainties source	Calculated uncertainties	Evaluation\comments
Optical density measurements	0.78%, 0.80% and 1.12%	Uncertainties in red and green channels and combined uncertainty
Exposure time: (4-38) hours	<1.00%	Clock was used to keep record of exposures
Activity measurements	5.82%	Combined uncertainty of activity concentration and dose calibrator uncertainty
Curve fitting	2.20%, 3.61% and 4.22%	Uncertainties in red and green channels calculated and combined uncertainty
Measurement of absorbed dose	4.56%	Combined uncertainty resulted from the red and green channels
Overall uncertainty	8.64%	Combined uncertainty from all individual components

Accepted Article

Table 2. Densities and atomic compositions of the materials used in this work are following:

Material	Density (g/cm <sup>3</sup> )	C	O	H	N	Ca	Cl	Other
Lung	0.307	60.06	22.98	8.30	2.76	0.00	1.08	Mg: 4.77
Cortical bone	1.898	29.40	38.90	2.60	0.80	26.10	0.03	Al: 2.10

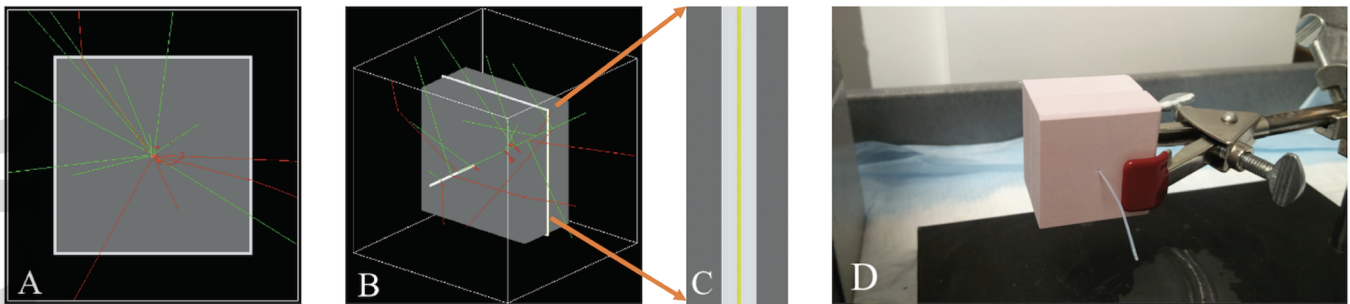
Source: Computerized Imaging Reference Systems (CIRS) Inc. 2019

Table 3. Composition of different layers of EBT3 films:

EBT3 film	Density (g/cm <sup>3</sup> )	C	O	H	Li	Other
Active layer	1.20	27.60	13.30	56.80	0.60	Al: 1.60
Polyester layer	1.35	45.50	18.10	36.40	0.00	K: 0.00

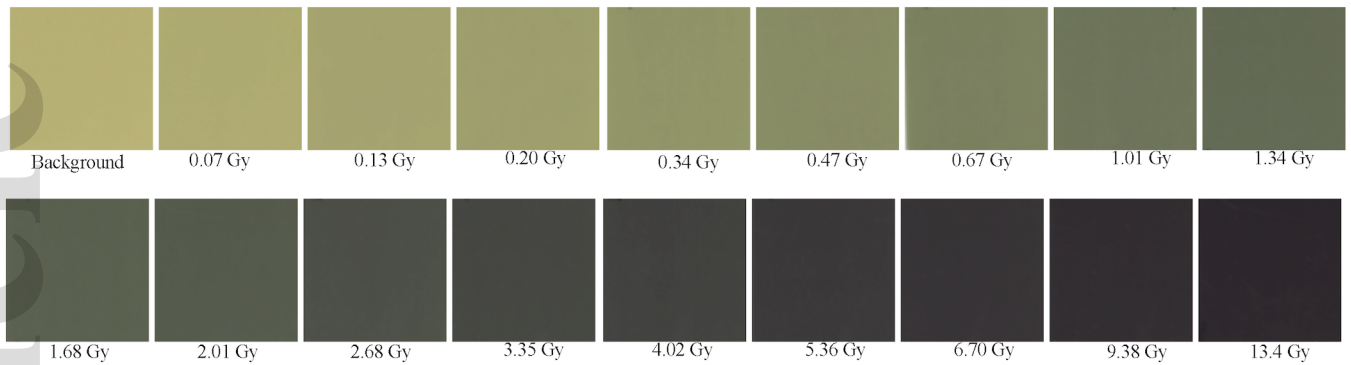
Source: Atomic compositions and mass densities of materials were taken from the data provided by the manufacturer.

Accepted Article

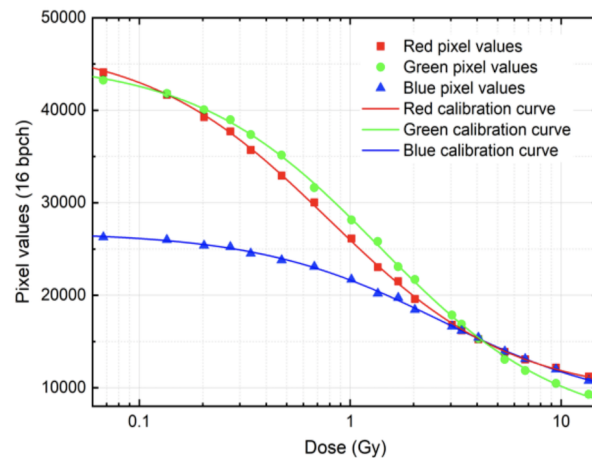


mp\_14463\_f1.tif

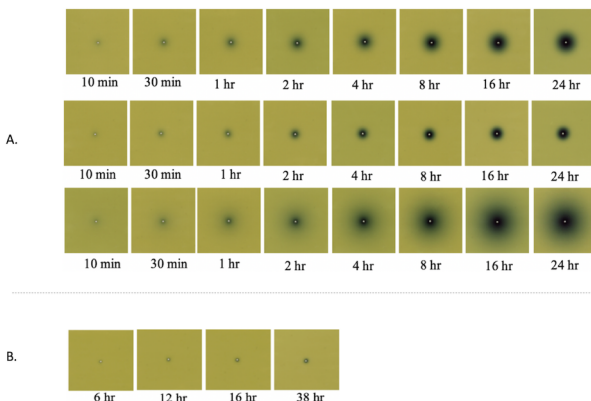
Accepted Article



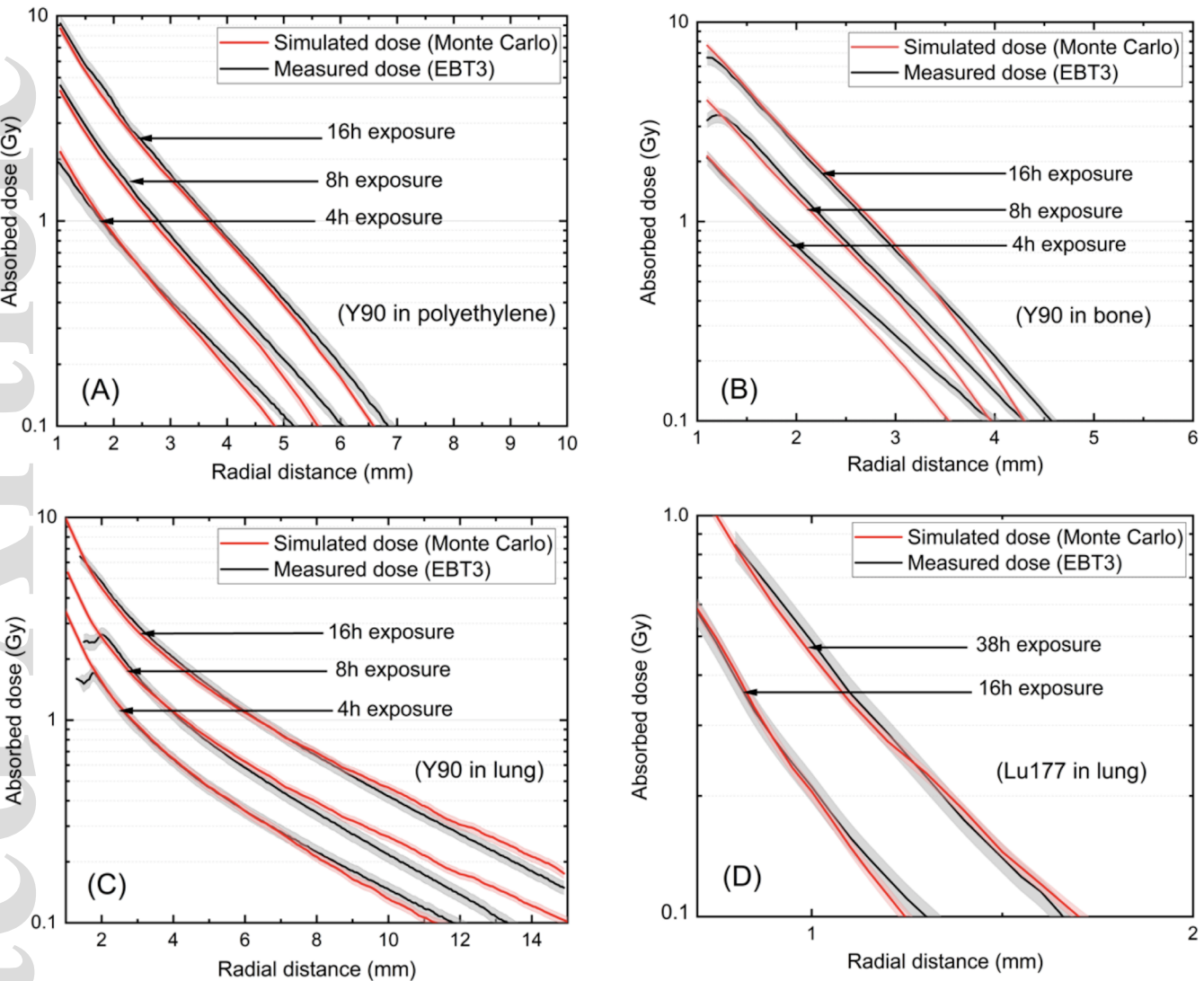
mp\_14463\_f2.tif



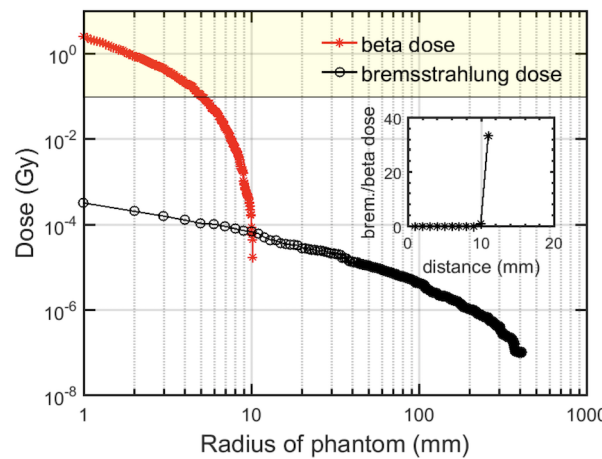
mp\_14463\_f3.tiff



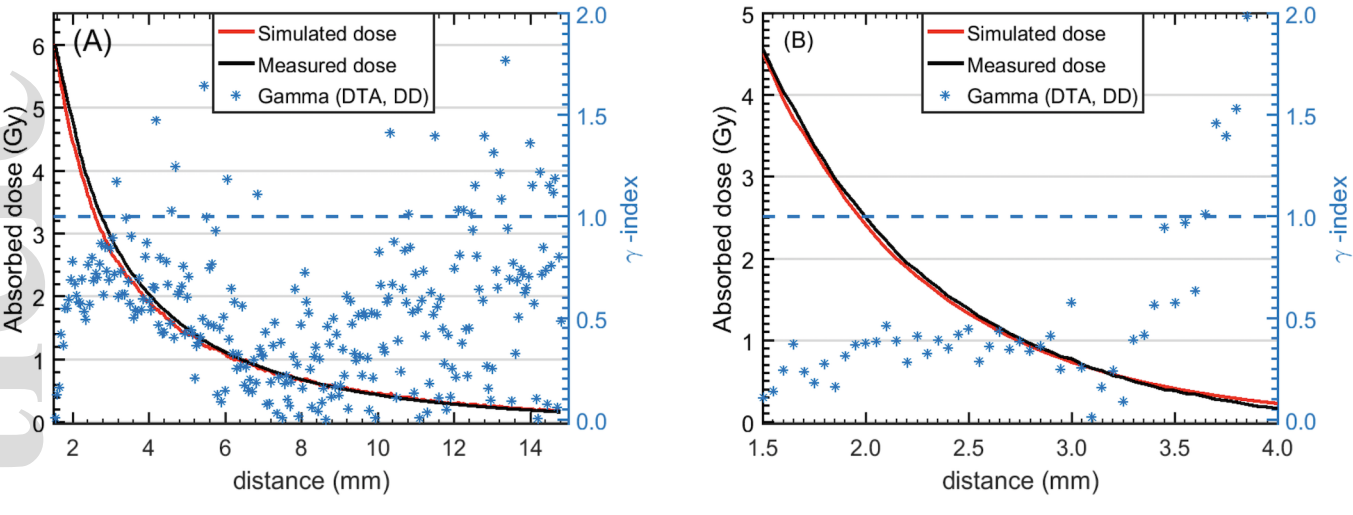
mp\_14463\_f4.tif



mp\_14463\_f5.tif



mp\_14463\_f6.tiff



mp\_14463\_f7.tif